RSC Advances

PAPER

View Article Online
View Journal | View Issue

Cite this: *RSC Adv.*, 2021, **11**, 22517

pH-responsive viscoelastic supramolecular viscosifiers based on dynamic complexation of zwitterionic octadecylamidopropyl betaine and triamine for hydraulic fracturing applications†

Shuhao Liu, ‡[a] Yu-Ting Lin, ‡[a] Bhargavi Bhat,[a] Kai-Yuan Kuan,[d] Joseph Sang-Il Kwon[ac] and Mustafa Akbulut *[abc]

Viscosity modifying agents are one of the most critical components of hydraulic fracturing fluids, ensuring the efficient transport and deposition of proppant into fissures. To improve the productivity index of hydraulic fracturing processes, better viscosifiers with a higher proppant carrying capacity and a lower potential of formation damage are needed. In this work, we report the development of a novel viscoelastic system relying on the complexation of zwitterionic octadecylamidopropyl betaine (OAPB) and diethylenetriamine (DTA) in water. At a concentration of 2 wt%, the zwitterionic complex fluid had a static viscosity of 9 to 200 poise, which could be reversibly adjusted by changing the suspension pH. The degree of pH-responsiveness ranged from 10 to 27 depending on the shear rate. At a given concentration and optimum pH value, the zwitterionic viscosifiers showed a two-orders-of-magnitude reduction in settling velocity of proppant compared to polyacrylamide solution (slickwater). By adjusting the pH between 4 and 8, the networked structure of the gel could be fully assembled and disassembled. The lack of macromolecular residues at the dissembled state can be beneficial for hydraulic fracturing application in avoiding the permeation damage issues encountered in polymer and linear-gel-based fracturing fluids. The reusability and the unnecessary permanent breakers are other important characteristics of these zwitterionic viscosifiers.

Received 12th January 2021
Accepted 26th May 2021

DOI: 10.1039/d1ra00257k

rsc.li/rsc-advances

Introduction

Even though there is rapid development in renewable energy technologies, oil and natural gas still play a critical role worldwide for residential uses, commercial and industrial applications, power generation, and transportation; and are irreplaceable as raw materials for chemical reactions and material synthesis. In a recent study, the U.S. Energy Information Administration (EIA) reported that petroleum and natural gas accounted for 69% of the primary energy consumption of the US in 2019.[1] Similar trends were also observed globally: natural gas and oil were used to satisfy about 54% of the world energy demand in 2019.[2] While the volume of proven global shale gas is predicted to be 7299 trillion cubic feet, the amount of proven shale oil is estimated to be 335 billion barrels in the world.[3] As the global population and industrialization level increase, so is the energy need. To meet this demand, hydraulic fracturing has increasingly been relied upon. The US natural gas production by the hydraulically fractured wells increased from 7% in 2000 to 67% in 2015.[4] Meanwhile, the US crude oil production from hydraulically fractured wells increased from 2% in 2000 to 51% in 2015.[5] In terms of global shale gas production, the shale gas production in 2040 was projected at 168 billion cubic feet per day compared to 42 billion cubic feet per day in 2015, corresponding to a 400% increasing in 25 years.[6]

The hydraulic fracturing process injects several million gallons of fluid containing proppants such as sand or ceramic at high pressure to create fissure and crack in the shale.[7,8] The proppants are left to keep the fissure and crack open to help the oil and gas flow freely. After releasing the pressure, fluid flows back from the well, which recovers not only the fracturing fluid but also the chemicals and resources from the reservoir.[9] During the procedure of injection and flow back to pipeline, viscosity is the key point to influence the recovery of oil or gas from the wellborn.[10] Typically, fracturing fluid contains 98% to 99.5% water and 0.5% to 2% chemical additive.[7] One of the most important components of fracking fluid is the viscosity modifying agent, which prevents

[a]*Artie McFerrin Department of Chemical Engineering, Texas A&M University, College Station, TX 77843, USA. E-mail: makbulut@tamu.edu*
[b]*Department of Materials Science and Engineering, Texas A&M University, College Station, TX 77843, USA*
[c]*Texas A&M Energy Institute, College Station, TX 77843, USA*
[d]*Department of Chemistry, Texas A&M University, College Station, TX 77843, USA*

† Electronic supplementary information (ESI) available. See DOI: 10.1039/d1ra00257k

‡ Both authors contributed equally to this work.

settling and non-homogeneous dispersion of proppant and provides a strong driving force on proppant to follow the fluid into cracks, fractures, and fissures.[90] Without viscosifying agents, it is impossible to adequately transport proppants from the surface to the fissures.[89,90] Currently, the lack of effective, reliable viscosifiers is a limiting factor causing sub-optimal permeability increases and relatively low productivity index in shale reservoirs even when other steps of hydraulic fracturing are successfully executed.

The commonly used viscosity modifiers are polymeric materials such as the polyacrylamide and its derivatives,[11,12] poly(vinyl alcohol),[13] poly(acrylic acid),[14] cellulose (such as carboxy methylcellulose and hydroxyethylcellulose),[15] and nature polymer guargum based materials.[16] Polymeric material has been successfully utilized in several reservoirs among different countries in the past decades.[17] However, polymer has several limitations when applied as fracturing fluid, decreasing production efficiency.[18] First, insoluble residue formation damages the formation by plugging the pore or pores throats.[19] Second, the plugged pores by the residue cause the reduction of formation permeability that reduces the mobility of oil and gas.[20] Moreover, these polymeric materials generally have poor resistance to heat and salinity in the reservoir and suffer shear degradation during the injection.[9]

Recently, surfactant-based aqueous viscoelastic fracturing fluids have been considered as a possible replacement for the polymeric materials in hydraulic fracturing fluids.[19,21] Based on the concentration and ionic strength of components as well as molecular architecture, self-assembly of surfactants forms micelles of varying shapes such as spherical micelles,[22] rod-like micelles,[23] vesicles,[24] and wormlike micelles (WLM).[25,89] Because of the formation of entanglement, overlap and networks, long and flexible WLM in an aqueous system exhibit excellent viscoelastic characteristics similar to the polymer solution but no residues.[26,27] Several researchers studied the clean fracturing fluid with high flow back rate, low friction, and low damage to the formation with the surfactant system. Chieng *et al.*,[28] reported a viscoelastic surfactant (VES) through mixing the traditional cationic surfactant cetyltrimethylammonium bromide (CTAB) with maleic acid and citric acid. VES based fluid showed good resistance to the temperature and shear by shearing at 170 s^{-1} at 90 °C for 2 hours. Besides, the gel could be easily broken by adding ethanol and exhibit a small core damage rate. Sun *et al.*[29] reported a CO_2 VES foam fracturing fluid prepared by C18 saturated alkyl trimethyl ammonium bromide and crosslinked by sulfosalicylic acid triethanolamine ester, which exhibited a heat resistance to higher than 120 °C.

Most of the prior studies have focused on the cationic or anionic surfactants as building blocks of viscoelastic surfactant systems.[27–31] Similar studies with zwitterionic surfactants, which have two distinct and oppositely-charged groups as a head-group, are limited in numbers. The assemblies of zwitterionic surfactants can exhibit a better thermal resistance than that of other surfactants and could be switched from nonionic to cationic or anionic by adjusting the pH.[30,32] Besides, the zwitterionic systems tend to show a high salinity resistance, enhanced biodegradation, and less sensitivity to divalent ions.[33–35] Compared to anionic and cationic surfactant, betaine type zwitterionic surfactants tend to have a better dispersibility and colloidal stability, once assembled, with respect to pH and salt. Furthermore, betaines containing carboxyl group exhibit a better water solubility in comparison to other types of zwitterionic surfactants such as betaine with sulfonate group.[34,36,37] Because of these characteristics, recently, betaine-type surfactants have gained increasing attention in the exploitation of natural sources as an additive in hydraulic fracturing fluids. For instance, Baruah *et al.*[32] reported the combination of CAPB and sodium oleate could yield viscoelastic systems with viscosity stability against high pressures. Dai *et al.*[33] reported the adsorption behavior and surface tension of zwitterionic cocamidopropyl betaine (CAPB) solution at temperature of 90 °C and salinity of 115 200 ppm. Wei investigated the combination of the CAPB with amino acid surfactant with different pH and temperature to gain insights into the interaction between CAPB and sodium lauryl sarcosinate.[38] However, the majority of research on zwitterionic viscoelastic systems has relied on CAPB; other zwitterionic structures have not been explored much; and the assessment of how such viscoelastic materials interact with proppant mostly lacks in the literature. Compared to short-chain CAPB, betaine type surfactants with long-chain have started to gain more attention in recent years because of the lower critical micellar concentration (CMC) of longer alkyl chains.[39,40]

Herein, we report a pH-stimuli viscoelastic system based on molecular complexation of zwitterionic octadecylamidopropyl betaine and diethylenetriamine in aqueous media and the evaluation of proppant carrying capacity under systematically varied conditions. Octadecylamidopropyl betaine was synthesized by the condensation reaction of stearic acid and dimethylaminopropylamine and the further condensation of the product with chloroacetic acid. The rheological properties of the developed viscosity system were investigated as a function of pH, temperature, and salinity, considering the reservoir conditions of various shale reservoirs. The proppant carrying capacity was measured *via* a sand-settling assays at a temperature of 25 °C and 90 °C and salinity of 0–5 wt%. The ability to control the retainment and settling of viscoelastic system was probed in the context of active and passive mechanisms under different pH conditions.

Method

Material

Aluminum oxide (Al_2O_3) (activated, neutral, 150 mesh), stearic acid (SA, 95%), chloroacetic acid and sodium chloride (NaCl) were purchased from Sigma Aldrich (St. Louis, MO). *N*,*N*-Dimethyl-1,3-propanediamine (DMPDA, >99%) and sodium fluoride (NaF, 99%), diethylenetriamine (DTA) were purchased from Alfa Aesar (Tewksbury, MA). Polyacrylamide was purchased from Sigma Aldrich (St. Louis, MO). All chemicals were used as received. Ultrapure water with a resistivity of 18.2 MΩ cm was collected from a water purification system (Millipore Milli-Q, Integral 10, Burlington, MA).

Preparation of dynamic binary complex (DBC) gels

The synthesis procedure of octadecylamidopropyl betaine (OAPB) was described in Fig. 1a. First, stearic acid was mixed with DMPDA

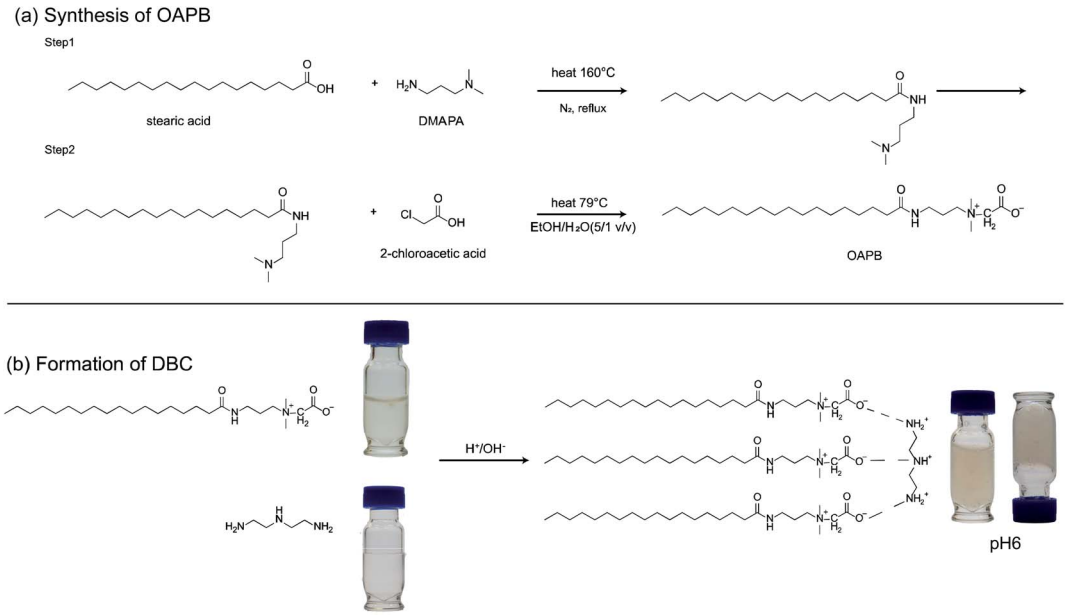

Fig. 1 (a) The reaction scheme for the formation of long-chain, large head-group zwitterionic amphiphile (OAPB) using stearic acid, DMPDA, and chloroacetic acid. (b) The supramolecular complexation of OAPB with triamine to yield viscoelastic gel.

at a molar ratio of 2 : 3 (SA : DMPDA) in a two-necked flask containing NaF catalyst and dehydration agent Al_2O_3. The components were allowed to react *via* refluxing at 160 °C for 10 hours in the presence of nitrogen gas as described elsewhere.[41] The resultant material, which is an amidoamine, was washed with acetone several times to remove unreacted materials and impurities, if any, and then vacuum dried at 40 °C for 24 hours. The yield of the amidoamine during the first step was determined to be to 85%. Afterward, amidoamine and chloroacetic acid at a molar ratio of 1.25 : 1 and total 30 grams were dissolved in 100 mL ethanol : -water solution (5 : 1 v/v), followed by adjustment of the solution to alkaline conditions with the addition of 0.5 M NaOH. The reaction was carried out with a reflux system under nitrogen atmosphere at 80 °C for 24 hours. Upon completion of the reaction, the final product consisting of a long-chain tail group and a large zwitterionic head group with a quaternary ammonium cation and a carboxylate anion was washed with ethyl acetate several times and then dried under vacuum at 40 °C for 24 hours. After vacuum drying, the weight of the product was measured which corresponding to an isolated yield of 75%.

By mixing the resultant zwitterionic amphiphile, OAPB, with triamine (DTA) at a molar ratio of 1 : 3 with a total active concentration of 2 wt% in water, a dynamic binary complex (DBC) with viscoelastic characteristics was produced (Fig. 1b). The suspension was homogenized *via* probe sonication for 10 minutes at a power of 2000 W and 20 kHz (SJIA-2000 W; Ningbo Haishu Sklon Electronic Instrument Co., Ltd., Ningbo, China). The suspension pH was adjusted by dropwise addition of 0.05 M H_2SO_4 and 0.05 M NaOH.

Chemical characterization

The intermediate and final compounds forming during various stages of reactions were investigated using attenuated total reflectance-Fourier transform infrared (FT-IR) spectroscopy (Nicolet iS5, Thermo Fisher Scientific, Waltham, MA). The FTIR spectra were obtained in the wavenumber from 400 cm^{-1} to 4000 cm^{-1} with 1 cm^{-1} step size and triplicate repeats. The captured spectra were analyzes using Omnic software suite (version 9.2.86, Thermo Fisher Scientific). In addition, the proton nuclear magnetic resonance scope (^{1}H NMR) was undertaken *via* a Varian VNMRS at 500 MHz. The ^{1}H NMR were obtained by dissolving amidoamine and OAPB in deuterated chloroform and deuterated methanol, respectively.

Rheological measurements

Shear viscosity characteristics of the resultant dynamic binary complexes were measured using a stress-controlled rheometer (Haake RheoStress 1, Thermo Fisher Scientific) with parallel-plate (20 mm titanium) geometry. In rheological studies, the main experimental variables studied were solution pH (from 2 to 12), temperature (25 °C, 45 °C, 65 °C, 95 °C), and salinity (0, 1, 3, 5 wt%). After DBC (2 wt% in water) at pre-determined conditions (pH, temperature, and salinity) was prepared, the suspension was left to equilibrate under these conditions for thirty minutes in a sealed container to minimize evaporation losses. Then, the rheological measurements were carried out at 1 mm gap with a shear rate varying between 10^{-2} and 10^{2} s^{-1}. For comparison purposes, a well-known viscosifying agent used in hydrocarbon recovery applications, PAM was selected. Each experiment was repeated at least three times to ensure statistical reliability and confirm reproducibility.

The same rheometer and geometer were used to determine the viscoelastic properties through dynamic oscillatory frequency sweep with a constant 1% strain from 0.01 to 10 Hz, which was in the linear viscoelastic regime of the sample at

25 °C. Before the frequency sweep, the samples at different pH, the linear viscoelastic regime was determined from dynamic strain amplitude sweep at room temperature with 1 Hz.

Proppant carrying capacity

To determine the proppant carrying capacity and average settling velocity of proppant in DBC gels, we relied on sand settling assay described elsewhere.[9] In these experiments, 7 wt% of 20–40 mesh sand, which was selected as model proppant, was placed in a 20 mL glass vial containing 20 mL DBC gel and rigorously shaken and vortexed to form a proppant dispersion. Right after the dispersion was placed on the laboratory bench, the settling behavior was captured with a digital camera (H-HAS12035, Panasonic, Japan). For the first 10 min, the video was continuously captured at a frame rate of 30 fps. Then, the images were captured once every two minutes between 10 min to 4 hours, and every 10 min after 4 hours until sand was 99% settled down. The average settling velocity was calculated by dividing the settling length (half of the vial height) by the settling time, which we define as the settling of 95% of sand particles detectable. Briefly, it was assumed that sand was homogeneous suspended in a vial, meaning there were initially equal number (number density) of sand particles near the top and the bottom. By further assuming that the acceleration effects are negligible (*i.e.*, settling velocity is constant), we calculated the average settling velocity using the mean distance of travelled by sand particles from the suspended state to the settled state (*i.e.*, the half-height of the sand column) and the critical settling time (until no sand grains can visually be detected). For more convenient visualization, we relied on sand with blue color (fine stone granules, Ashland, KY) after establishing that quartz sand behaves similar to blue sand in terms of settling behavior. Also, the sand was filtered with a 20–40 mesh filter to reduce large variations in the particle size. In these experiments, the influence of external factors such as salt concentration (from 0 wt% to 5 wt%), pH (4, 6, 8 and 10); and temperature (25 °C and 90 °C) on the proppant carrying behavior of DBC were evaluated. The time required for settling 95% of sand was taken as the critical settling time for these systems.

Zeta potential measurement and microstructural analysis

To gain insights into the interactions between proppant (sand) and DBC gels by measuring changes in the zeta potential of DBC gel and sand, we utilized electrophoretic light scattering technique (Zetasizer Nano ZS90, Malvern, Westborough, Massachusetts). The zeta potential was calculated from mobility *via* the Smoluchowski approximation,[42] which is valid when the Debye length is much smaller than the characteristics particle size (*i.e.*, thin double layer condition). Briefly, the zeta potential was calculated using the Henry equation: $U_E = 2\varepsilon z f(k_a)/3\eta$, where U_E is the electrophoretic mobility detected by M3-PALS technique, ε is the dielectric constant, η represents the viscosity of the solvent, ζ is the zeta potential and $f(K_a)$ is the Henry's function. Since the electrophoretic determination of the zeta potential is made in diluted aqueous media, $f(K_a)$ is 1.5 in this case according to the Smoluchowski approximation.[43] In our studies, the zeta potential values were conducted with the 2 wt% samples, sand in the ultrapure water and 2 wt% samples with sand at pH 2, 4, 6, 8, 10, and 12 since their assembly state and viscosity characteristics can change with concentration. The samples were vortex-mixed for 10 minutes to suspend the assembly well and then injected into the folded capillary cell DTS 1070 for the zeta potential measurements. The structural characteristics of DBC gels were probed using an optical microscope (BioRyx 200 system, Arryx Inc., Chicago) with 30× lens.

Results and discussion

Chemical characterization

The zwitterionic building block of DBC gel was obtained from stearic acid, which is one of the most common fatty acids that can be produced in sustainable fashion from coconuts. To confirm the condensation reaction of stearic acid with DMPDA and further condensation of the resultant compound with chloroacetic acid, we utilized FTIR spectroscopy (Fig. 2). The spectra revealed that the reaction of DMPDA with steric acid resulted in the shifting of peak at 1699 cm^{-1}, which is due to C=O stretch of carboxylic acid group (stearic acid), to 1638 cm^{-1}, which can be ascribed to the C=O stretch of amide

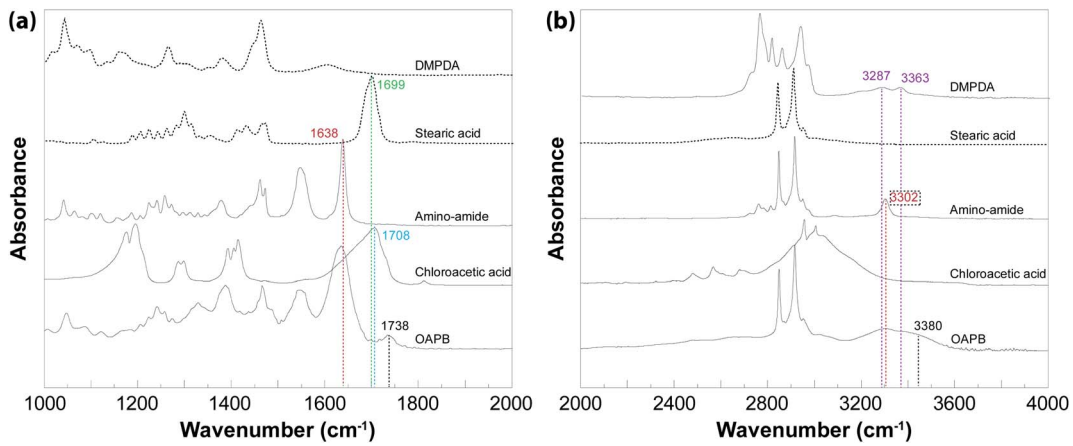

Fig. 2 FTIR of long-chain zwitterionic amphiphile and its reactants in the frequency range of (a) 1000–2000 cm^{-1} and (b) 2000–4000 cm^{-1}.

from the amino–amide intermediate. The observation of the amide peak indicates the successful production of the intermediate. On the amino-amide spectra, characteristic bands for N–H stretching of secondary amide, two C–H stretchings of long-chain alkane, and C=O group of vibration from secondary amide were found at 3307.8 cm^{-1}, 2846.8 cm^{-1}, 2915.8 cm^{-1}, and 1639.1 cm^{-1}, respectively. The product forming with the reaction of amino–amide with chloroacetatic acid was featured with two carbonyl peaks on its FTIR spectra with one due to the C=O stretching of original amide, RC(=O)NR′(1699 cm^{-1}), and another owing to the C=O stretching of carboxyl, R″HN–CH_2–C(=O)OH (1738 cm^{-1}). The appearance of the peak at 1738 cm^{-1} for OAPB compared to amino-amide can be attributed to the formation of RHN–CH_2–C(=O)OH group. The persistence of peak at 1638 cm^{-1} implies that amido group of aminoamide did not participate in the chemical reaction. The shift from 1708 cm^{-1} carboxylic group in chloroacetic acid to 1738 cm^{-1} in OAPB indicates a change of electronegativity of the neighboring atom due to the presence of positive charge from quaternary amine.[44] For the OAPB synthesized, other major peaks were identified to be C–H bending at 1461.7 and 1472.3 cm^{-1} and N–H bending at 1550.4 cm^{-1}.[45,46]

A similar analysis in the region of 2000 cm^{-1} to 4000 cm^{-1} revealed that primary amine of DMPDA had N–H stretching peaks at 3287 cm^{-1} and 3363 cm^{-1}. Upon reaction of DMPDA with stearic acid, these peaks shifted to 3302 cm^{-1}, which can be ascribed to the N–H stretching of amide forming (amino–amide). The reaction of chloroacetic acid with amino–amide resulted in the emergence of a shoulder at 3380 cm^{-1} which is likely to be because of the O–H stretching from carboxylic terminal group of OAPB.[47,48] Overall, when we put these pieces together, we can conclude the successful synthesis of OAPB as illustrated in Fig. 1. In addition, the complementary ^{1}H NMR results of OAPB and amidoamine were also represented in ESI Fig. S5† to further confirm the reactions.

Influence of pH on the viscosity of DBC gels

Fig. 3 compares the static viscosity (*i.e.*, zero frequency) values of DBC involving OAPB and DTA and PAM, which is a commonly used viscosifier in fossil fuel recovery applications at the same concentration (2 wt%). Based on these data, the following observations can be made: First, DBC provides a superior thickening characteristic as a viscosity modifier compared to PAM for all pH values. Above pH 10 and below pH 6, the DBC solution was about five-orders-of magnitude more viscous than water. Second, while viscosity of PAM was mostly constant with respect to pH, DBC demonstrated a strong variation in viscosity with pH. The ratio of the maximum and minimum static viscosity was about 26.9 for DBC while the ratio was 2.4 for PAM. The viscosity of DBC at pH 8 was significantly smaller than that at pH values above 10 and below pH values 6. Several forces dominated among the DBC, including electrostatic force, hydrogen bonding, and hydrophobic interactions. The switchable viscosity can be ascribed to the differing extent of protonation and deprotonation for carboxyl terminal group of OAPB and amine groups of DTA at different pH values. The state of protonation and deprotonation of these building blocks controls hydrogen bonding and electrostatic interaction and therefore the assembly dynamics. Similar pH-responsive behavior for complexes involving other types of carboxylic acids and amines have been reported in past studies.[49–51] Briefly, the charge of OAPB and DTA depends on the pH of the solution and the electrostatic attraction between them occurs once opposing charges appear on them at the same time. At low pH, the DTA protonated (+3 or +2) to combined with the deprotonated OAPB to form more ordered orientation and become tightly-packed.[9,52] Also, the C=O group of OAPB and neutral N–H group of DTA can help the hydrogen bonding formation contribute to the network structure formation.[53] Thus, the electrostatic attraction, hydrogen bonding and the hydrophobic force between long carbon chain can contribute to the assembly and hence, improved viscosity. However, after pH becomes neutral (pH 7–8), the electrical attraction becomes weaker and the number of non-bonded OAPB increased due to the decrease in the protonation of DTA, which can not only generate free amphiphiles but prevent the formation of micelles. This causes the low viscosity and small phase-separation. On the other hand, at the high pH, the DTA become neutralized; thus, the electrostatic attraction was diminished, but the hydrogen bonding was strengthened. The net charges of DBC were low and the main driving forces for DBC were hydrogen bonding and hydrophobic interactions that contributed to tight and ordered structure again. The repulsion between quaternary ammonium was screened by the carboxyl group of OAPB and OH– in the solution. Thus, the viscosity started increasing compared to the neutral condition. Overall, pH-responsiveness is the key feature of DBCs making them attractive as fracturing fluid viscosifiers which is to satisfy on-demand need for carrying and depositing proppants during the stimulation step.

Influence of shear rate and temperature on the viscosity of DBC gels

The volumetric flow rates of hydraulic fracturing injection changes from well to well and from service company to service company. Accordingly, it is important to have a comprehensive

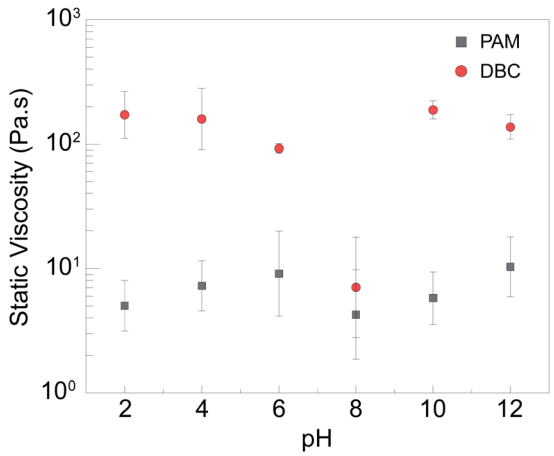

Fig. 3 Static (*i.e.*, zero-frequency) viscosity of DBC suspension (2 wt%) involving OAPB and DTA building blocks and PAM (2 wt%) as a function of pH at 25 °C. Error bars indicate the relative error of static viscosity for three repetitions.

understanding of how the viscosity of DBCs changes with shear rate if they would be used as fracturing fluids. In addition, temperature is an important parameter that must be considered in the context of viscosifier performance owing to the geothermal gradient.[54,55] Fig. 4 shows the dependence of viscosity of DBCs to shear rate and temperature for pH values from 2 to 12. For all samples, viscosity decreased with increasing shear rate, indicating a shear-thinning behavior. However, the DBCs retained their viscous characteristics and were two-to-three orders of magnitude more viscous than water even at extremely high shear rates. Shear-thinning behavior can be ascribed to the shear-induced ordering of DBC chains and/or the disruption of dynamical assembly and disassembly equilibrium of building blocks of DBC. Furthermore, it is important to underline that polymers, such PAM, tend to degrade under higher shear rate, which limits their applications as reusable viscosity modifiers in this area.[9,56,57] On the other hand, DBCs returned to their high viscosity states once the shear rate is reduced, indicating the lack of permanent damage.

Regarding the influence of temperature on the viscosity of DBC, as temperature increased, the viscosity mostly decreased (Fig. 4). However, once the temperature exceeded 65 °C, the viscosity increased with temperature at pH 2 and 4 (Fig. 4d). This may be attributed to the increased solubility of long-chain fatty acids in water at elevated temperature and the resultant increased availability for complex formation.[58,59] Briefly, the increased solubility of OAPB enhanced the chance of DBC assembly because of raised possibility of interaction through electrostatic force between OAPB and triamine and might enforced network at low pH conditions. This type of trend was presented by some other studies of different type of VES.[60] It also maybe because of the restructuring of the micelles or reorganization of the counter ions near the micelles at different temperature.[60,61] On the other hand, the electrostatic attraction is strongest at the pH 2 and pH 4 due to the full protonation of DTA which may contribute to the stability of DBC to the high temperature.[34] Namely, a transformation from micellar state to free state can happen at the elevated temperature and free amphiphile can more readily partake in the assembly process.[62] It is also important to underline that even though viscosity mostly decreased with increasing temperature, the DBC suspension still had a better viscosity performance than PAM solution (shown in ESI Fig. S2†).

To better understand the influence of temperature on the viscosity of DBC and put its temperature sensitivity into a perspective compared to other types of viscosifiers, the relationship between temperature and viscosity was described by Arrhenius equation, $\mu(T) = \mu_0\, e^{(E_a/RT)}$.[63] Here, μ_0 is the viscosity at a reference temperature and E_a is the activation energy. The activation energy can be calculated from the slope of $\ln(\mu)$ *versus* $1/T$ plot. Fig. 5 shows the relationship between natural logarithm of zero-frequency viscosity and inverse of temperature. The linear regression analysis revealed that the activation energy

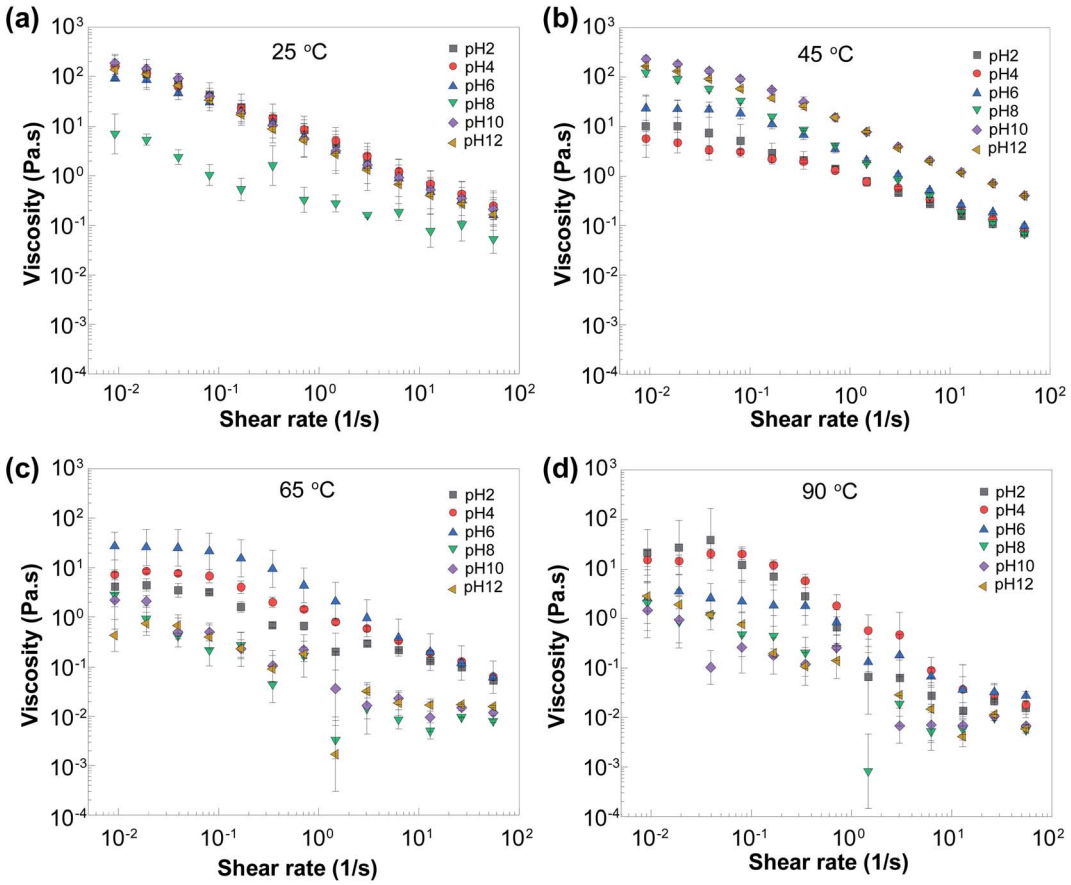

Fig. 4 The effect of temperature on the viscosity of DBCs (2 wt%) at (a) 25 °C, (b) 45 °C, (c) 65 °C, and (d) 90 °C for pH values of 2, 4, 6, 8, 10, and 12. Error bars indicate the relative error of viscosity for three repetitions.

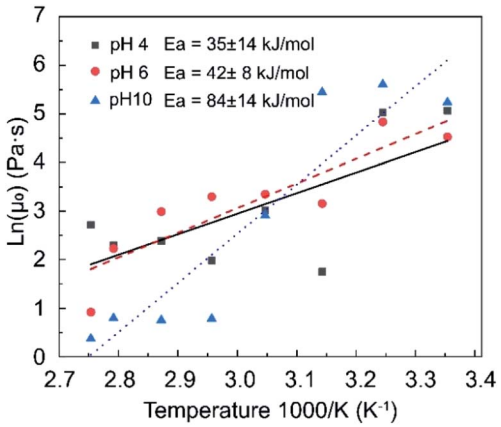

Fig. 5 Natural logarithm of static viscosity *versus* inverse temperature for DBC suspension.

was 21–49 kJ mol^{-1}, 34–50 kJ mol^{-1}, and 70–98 kJ mol^{-1} at pH 4, 6, and 10, respectively. In comparison to the weakly cross-linked PAM hydrogel presented by Du and Hill,[64] the disentanglement activation energies of their PAM was 15–60 kJ mol^{-1}. In this case, the DBC with pH 4 and pH6 has competitive performance with traditional polymer hydraulic system. Given that a lower activation energy indicates less sensitivity to temperature, as pH of DBC increases the temperature sensitivity increases. In comparison, activation energy for wormlike micelles were reported to be in the range of 70–300 kJ mol^{-1},[65,66] indicating that a better temperature tolerance of DBCs compared to wormlike micelles and also implying potential nanostructural differences between DBCs and wormlike-micelles.

Effect of salinity on the viscosity of DBCs

Seawater is often used as a source of solvent dispersing viscosifiers in fracturing fluids. The average salinity of seawater throughout the world is about 3.5%, with sodium chloride being the most abundant salt in it.[67] In addition, shale reservoir stimulated by hydraulic fracturing fluids tend to contain connate water with relatively high salinity.[68] Prior research indicated some of viscosifying agents such as wormlike micelles lose their viscous characteristics significantly in the presence of salts.[69,70] Similarly, polymer viscosifiers can degrade in the presence of salts.[71] For many supramolecular systems, the addition of salt in a solution causes the electrostatic screening and affects the pK_a in a rational manner that influences the polymerization or network structure formation.[72] As such, it is essential to study and understand how salinity influence the viscosity of DBCs to properly assess its potential as hydraulic fracturing fluid viscosifiers.

Fig. 6 demonstrates the viscosity as a function of shear rate at varying salinity conditions and pH values. At pH 4 and 6, the

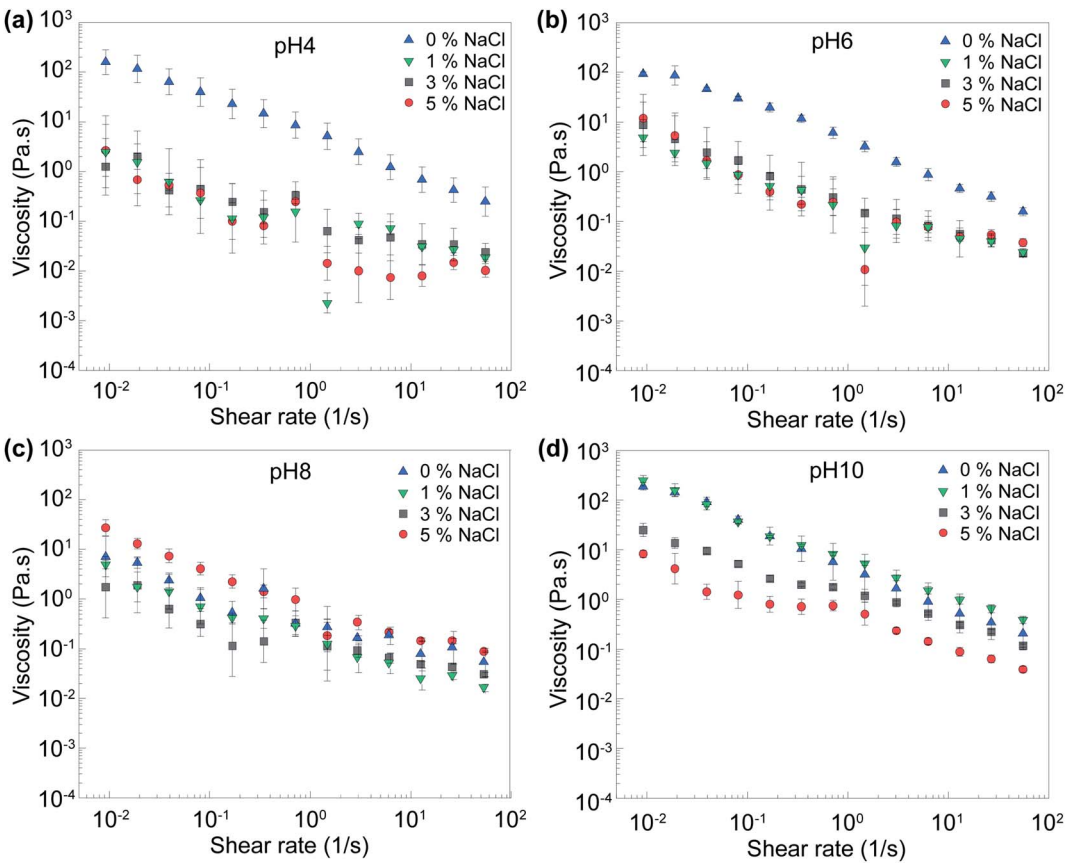

Fig. 6 Viscosity of DBCs (2 wt%) with respect to shear rate at different salinity value for (a) the suspension pH of 4, (b) the suspension pH of 6, (c) the suspension pH of 8, and (d) the suspension pH of 10. Error bars indicate the relative error of viscosity for three repetitions.

introduction of 1 wt% NaCl into DBC suspension in water reduced the static viscosity about 2.8–5.5 folds, but further salt additions did not further alter the viscosity significantly (Fig. 6a and b). At pH 8, the addition of small amount of salt (1 wt% and 3 wt%) slightly reduced the viscosity while the addition of 5 wt% salt increased viscosity by 2- to-4- folds (higher at lower shear rates). At pH 10, the addition of small amount of salt (1 wt%) did not modify the viscosity behavior much. However, when higher amount of salt (3 wt% and 5 wt%) is added, the viscosity decreased to lower and lower values. In comparison, the presence of salts only slightly reduced the viscosity of PAM solution. However, at a given viscosifier condition, the viscosity of DBCs were always larger than that of PAM solution. Conversely, the relative reductions in viscosity compared to no salt conditions were higher for DBCs. Hence, in the context of hydraulic fracturing, the following considerations can be made: the primary goal of fracturing fluid is to effectively carry proppant from surface to the fissures *via* borehole. For this step, it is required to have high viscosity and proppant carrying capacity.[73,74] Once proppant is forced and injected into the fissures, the viscosity has to be reduced to selectively pull water back but not proppant.[73] Connate water (high salinity) in shale reservoir is more likely to mix with the injection fluid at this last step. Hence, after proppant is deposited in the fissures, the reduction of viscosity can be beneficial in the context of selectively removing water back.

Regarding the nonlinear influence of salinity on the viscosity of DBC, the formation of dynamic binary complex involves intermolecular interactions such as electrostatic interactions and hydrogen bonding at multiple length scales. The presence of salts can weaken the strength of intermolecular bonds holding the nanostructured assembly together *via* the screening of electric fields.[75] The hydrogen bonding potential of uncharged surface groups of DTA and OAPB can also be reduced in the presence of salts. In addition, the presence of salts can also change the solution pH: the pH of acidic solutions tends to decrease upon addition of neutral salts.[76] Hence, the system can shift from one pH state to another pH state by adding salt. Another issue to consider is that the viscosity of water itself can increase when salt is added.[77] In addition, the distribution of hydrated salt ions near and within DBC assemblies can perturb structural order sterically similar to analogous supramolecular assemblies.[78,79] The sophisticated combinations of these molecular processes are likely to be responsible for the observed trends in viscosity in the presence of salt.

Breaking mechanism

The breakage of viscosifier after the use is an important element of hydraulic fracturing. The heuristics recommend that the viscosity of the broken gel should be lower than 5 cP to selectively remove the fluid without disturbing proppant. This viscosity value can be achieved with DBC at pH 10 for the typical reservoir conditions involving a shear rate over 100 s^{-1} (in porous media) and temperature of 90 °C according to the shear testing. On the other hand, the viscosity of DBC was measured at 90 °C by NDJ-9S digital rotational viscosity Meter that has a measurement range from 1 cP to 60 000 000 cP. The viscosity of DBC at pH 8 and pH 10 was both 4 cP at 90 °C. Hence, breaking can be induced by increasing pH, natural reservoir temperatures and high shear rates occurring in porous media may yield low viscosity values. Regarding the mechanism, the breaking takes place due to the disassembly of DBC, which are hold together *via* the interplay among van der Waals, electrostatic, and hydrogen bond interactions. The protonation and deprotonation state of molecular groups of short amines and zwitterionic, long-chain amphiphile change depending on pH. At higher pH values, amine group loses its proton (loses its positive charged) and cannot strongly interact with zwitterionic, long-chain, amphiphile.

Viscoelastic characteristic of DBC

Viscosity alone is not accurate enough to evaluate the proppant transportation behavior for the fracturing fluid. The proppant stability is also affected by the elastic property of the fluid which corresponding to the network structure of the material at microscales.[80] Thus, the linear viscoelastic region was determined from strain amplitude test and the oscillatory frequency sweep was conducted with constant 1% strain within the linear viscoelastic regime of the sample at 25 °C to understand the DBC gel at different pH better.

The strain sweep results were presented in the Fig. 7 and S8 (ESI†). A linear viscoelastic region (LVR) were observed for the pH 2 to 6 and pH 10 to 12 and has a larger G' compared to G'' in this region. Among them, we could figure out the similar behavior between pH 2 to 6. Besides, the DBC pH 10 and pH12 were similar. The DBC gels show the gel-like or solid structure before the structure breakdown at 2%, according to the LVR results at the experiment conditions. Further, the frequency sweep results at a range of 0.01 Hz to 10 Hz were shown in Fig. 8 and S9 (ESI†). The pH 2, 4, and 6 and pH 10 and 12 showed a similar property that a larger G'' compared to G' at frequency lower than 0.03 Hz that related to plastic material. Meanwhile, G' started being larger than G'' after 0.03 Hz represent an elastic

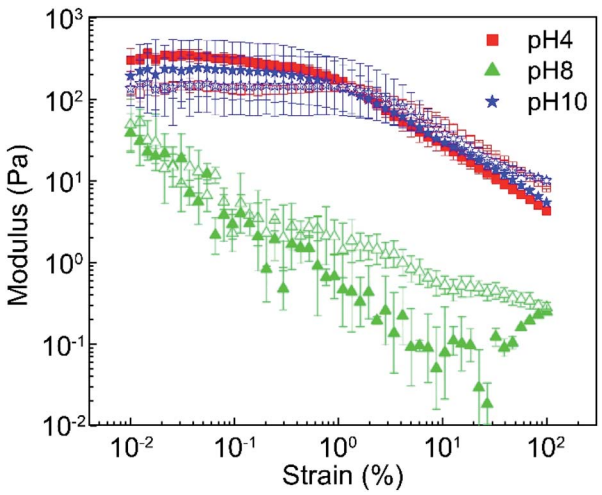

Fig. 7 The strain amplitude results show storage modulus G' (solid) and loss modulus G'' (empty) of DBC at pH 4, 8 and 10 with various strain (%) at 1 Hz.

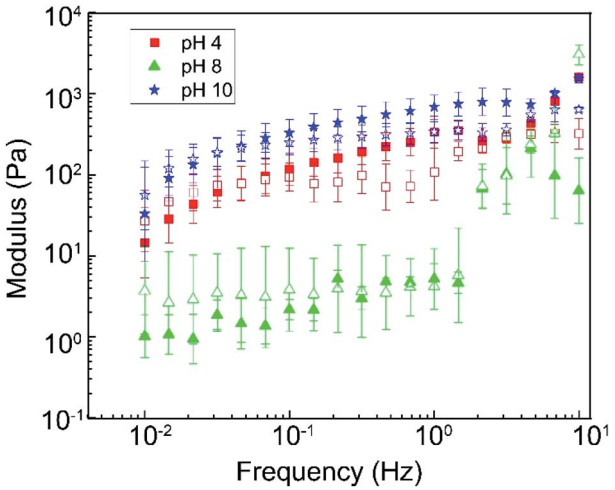

Fig. 8 The storage modulus G' (solid) and loss modulus G'' (empty) of DBC at pH 4, 8 and 10 with various frequency.

material. This trend is similar to many viscoelastic gel system reported by several studies.[34,35,81] On the other hand, the DBC at pH 8 performed as plastic (fluid material).

Proppant carrying capacity

Proppant carrying capacity is one of the most critical metrics used to evaluate the potential and efficiency of fracturing fluids.[82,83] Accordingly, we conducted sand settling studies to determine how the DBCs perform in terms of their ability to transport proppant at varying pH, temperature, and salinity conditions. Fig. 9 displays the images of sand suspension in DBC formulations in a time-resolved fashion. At room temperature, the complete settling of sand took place within 5 second for the solution pH of 8 while no settling was observed within 8 hours at pH 4, 6, and 10 (Fig. 9a). In comparison to DBC formulation (2 wt%), significant settling was noted after 10 minutes for PAM solution (2 wt%). The critical settling time, which we define as the time required for 95% of proppant to settle, was 1 day, 4 days, and 7 days at pH 10, pH 6, and pH 4, respectively. This means that the hydraulic fracturing fluid relying on DBC can be injected to the reservoir at initially acidic (pH < 6) or basic (pH > 10) conditions to have high proppant carrying ability.

In addition, the proppant carrying capacity studies at elevated temperatures (90 °C) revealed that the highest carrying capacity can be achieved at pH 4 (Fig. 9b). In terms of performance, the proppant carrying capacity at pH 6 was slightly lower than that at pH 4. The temperature significantly reduced the proppant carrying capacity at pH 10 where the critical settling time decreased from one day to a few seconds upon heating the system from 25 °C to 90 °C. The settling behavior was similar at 90 °C for pH 8 and 10. For the case of PAM solution, the proppant rapidly settled in PAM at 90 °C similar to at room temperature.

To be more quantitative, the mean settling velocities were calculated by analyzing the captured videos (Fig. 10). At room temperature (25 °C), the sand settling velocity in DBC solution was 6.58×10^{-8} m s^{-1}, 1.07×10^{-7} m s^{-1}, 5.25×10^{-3} m s^{-1}, and 3.93×10^{-7} m s^{-1} for solution pH 4, pH 6, pH 8, and pH 10, respectively. On the other hand, the mean settling velocity at

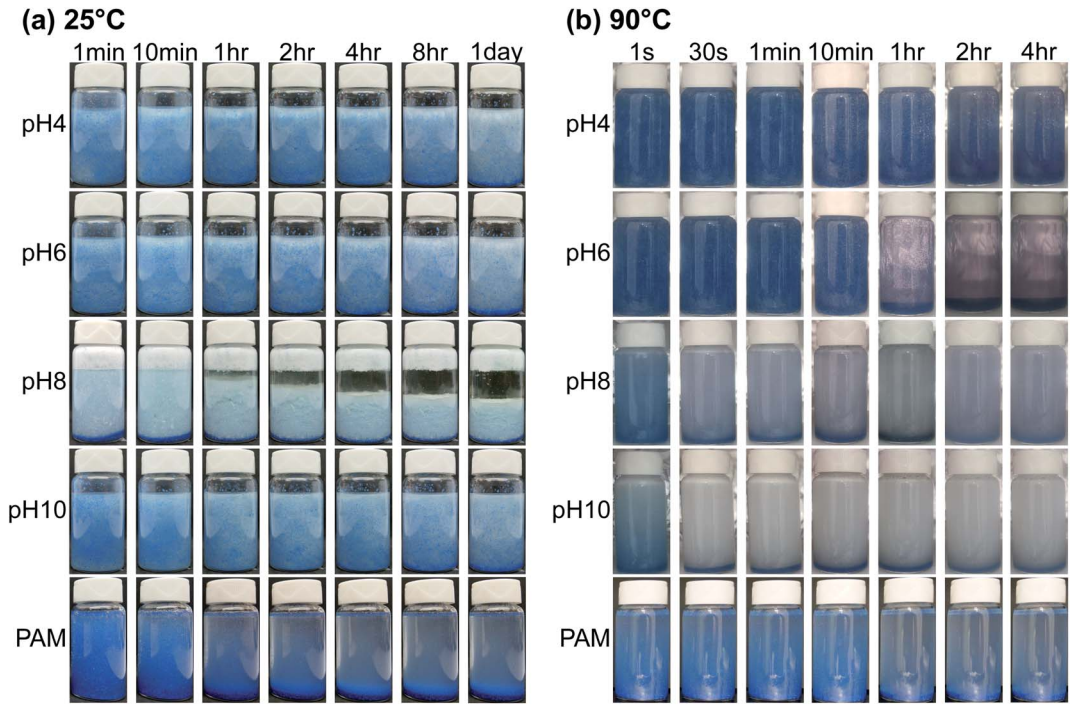

Fig. 9 (a) Sand settling in DBC solutions of pH 4, pH 6, pH 8, pH 10 with time at room temperature (25 °C). (b) Sand settling in DBC solutions of pH 4, pH 6, pH 8, pH 10 with time at higher temperature (90 °C).

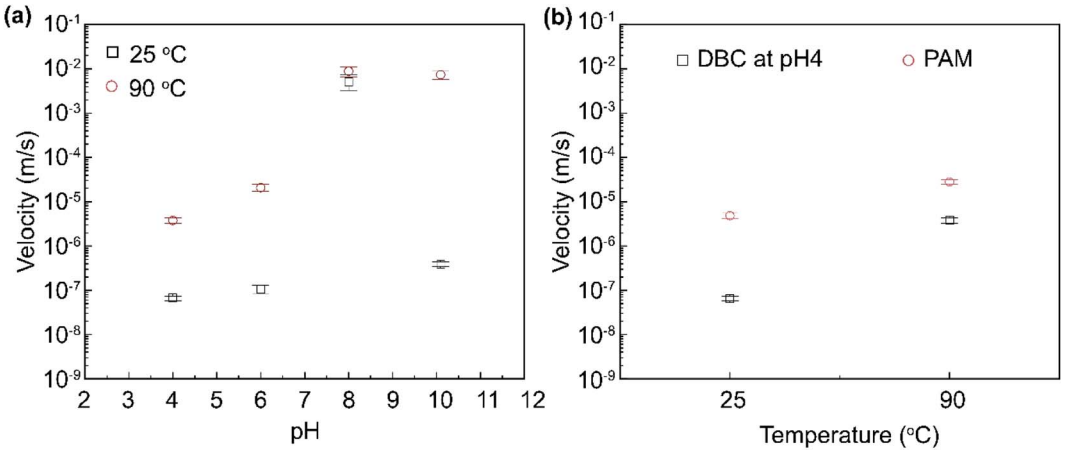

Fig. 10 (a) Settling velocity of sand in DBC suspension as a function of pH at 25 °C and 90 °C. (b) Comparison of sand settling velocity of DBC suspension and PAM solution (pH 4) at 25 °C and 90 °C. Error bars indicate the standard deviation for three repetition.

elevated temperature (90 °C) were about two to four orders of magnitude larger: 3.77×10^{-6} m s^{-1}, 2.0×10^{-5} m s^{-1}, 8.75×10^{-3} m s^{-1}, and 7.28×10^{-3} m s^{-1} for pH 4, pH 6, pH 8, and pH 10, respectively. Prior research reported that sand settling velocities below 8.0×10^{-4} m s^{-1} to 8.0×10^{-5} m s^{-1} is ideal for hydraulic fracturing applications.[34] Hence, it can be claimed that dynamic binary complexes demonstrate excellent sand carry capacity even at elevated temperatures for the conditions of pH 4 and 6.

Obviously, upon deposition of proppant into the fissures, it is needed to have very high settling velocity to separate water from the deposited proppants.[84] This can be achieved by adjusting pH of fracturing fluid from acidic conditions to basic condition by alkaline solution injection. Furthermore, the settling velocity of sand proppant was one to two orders of magnitude larger in PAM solution (slickwater) compared to DBC solutions at its optimum pH conditions (Fig. 10b). There are several reasons can be considered that may explain the lower settling velocity at pH 4 compared to the pH 6. The sand carrying capacity depends on the viscosity as well as the interaction between entangled network of the DBC and sand. Based on the viscosity data, it can be seen that viscosity is lower at pH 6 compared to pH 4. Next, one can look into the interactions rather than the viscosity to explain the enhanced proppant carrying capacity at pH 4. Namely, how the colloidal interactions between DBC and sand changes with pH should be considered in this context. The magnitude of electrostatic double-layer attraction/repulsion can change depending on and the dissociation nature of surface groups. It is also possible that the attractive van der Waals interactions between these colloidal entities can vary with pH. The dielectric constant of water decreases with the addition of salt/electrolytes. Hence, the dielectric constant of water is lower at pH 4 as more acid is added compared to pH 6. Based on the Lifshitz theory, the Hamaker constant of the system A (DBC/Water/Sand) in the aqueous suspension at pH 4 is lower than that at pH 6. As such, one possibility for the enhanced carrying capacity at pH 4 is increased van der Waals interactions. In addition, the dimensions (diameter) of DBC assemblies can also change with pH. The van der Waals forces, which are body forces, can also vary in this fashion.

In addition, Fig. S10 (ESI†) shows the relationship between the zero-shear viscosity of DBC *versus* the sand settling velocity. From these results, the slow settling of the sand in DBC with higher viscosity. However, there is not simply linear or reciprocal relationship between the viscosity and velocity. This could be explained that the sand stability in the micelle-based viscoelastic fluid not only affected by the viscosity, but also by the viscoelastic, microstructure networks, interaction between the sand and solution.[9,85,86]

As stated earlier, salinity is another parameter that needs to be considered in the context of hydraulic fracturing performance. Fig. 11 shows the influence of salt on the settling velocity of sand in at 90 °C as a function of pH (see ESI, Fig. S4,† for further details). It was found that the addition of salt did not noticeably alter the mean velocity of settling at pH 6 while the mean settling velocity in the presence of salt was about 2-fold

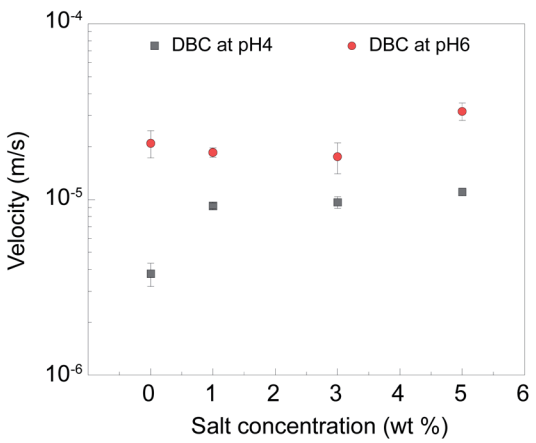

Fig. 11 The mean settling velocity of sand proppant as a function of salt concentration for the cases of pH 4 and pH 6 at 90 °C. Error bars indicate the standard deviation for three repetitions.

Fig. 12 Optical micrograph of a sand grain in DBC solution (a) at pH 4 and (b) at pH 8. (c) Zeta potential of sand in water, DBC suspension, and sand (divided by 20 to better show differing scales) in DBC suspension as a function of pH. The long, surface-aligned tubules (yellowish color) that are the supramolecularly assembled dynamic binary complexes localizing near the sand grain. Compared to pH4, the DBC solution at pH 8 contains no long tubules but large aggregates separated from the sand grain. The error bars indicate the standard deviation of triplicate measurements (see ESI† for larger images).

higher than that in the absence of salt at pH 4. Regardless, for the case of pH 4, DBC suspension could still retain desirably low settling velocities at 0.4×10^{-5} m s^{-1}, 0.9×10^{-5} m s^{-1} and 1.0×10^{-5} m s^{-1}; and 1.1×10^{-5} m s^{-1} at a salt concentration of 0, 1, 3, 5 wt%.

Interactions between sand proppant and dynamic binary complexes

To gain further insights into the reasons behind enhanced proppant carrying capacity of DBCs, we relied on zeta potential measurements and optical microscopy characterization (Fig. 12). It was found that DBC at pH 4 features long, yellowish tubules having a diameter of a few micrometers, much larger than that of wormlike micelles (Fig. 12a). Furthermore, it was clear that the local concentration of DBC chains was much higher near sand, indicating the favorable interactions between sand and DBC (see Fig. S6, ESI† for larger images). On the other hand, at pH 8, such long microscopic tubules were absent in the system, which can account for the lower viscosity value at these conditions (Fig. 12b). In addition, no adsorption or localization of DBCs near sand was also observed at this condition.

As can be seen from Fig. 12c, zeta-potential measurements revealed that proppant sand carries negative surface charge groups, presumable due to the dissociation and deprotonation of silanol and silicilic acid groups of quartz sand. The zeta potential increased with increasing basicity, which can be attributed the electron accepting nature or acidity of silanol and silicilic acid groups. DBC suspension had an isoelectric point between pH 8 and 10 (for further details, see ESI, Fig. S7†): the DBC assemblies had more cationic surface groups below pH 8 and more anionic surface groups above pH 10. These trends can be explained by the formation of more positive charges on the DBC tubules owing to the protonation of amino groups from DTA, the lower degree of dissociation for carboxylic groups under more acidic conditions, and the higher extent of protonation of tertiary amine group of OPAB. Hence, below pH 8, the electrostatic interactions between sand and DBC is attractive. *Via* zeta-potential measurements, the conjugation of DBC and sand upon mixing was also confirmed. It is known that proppant carrying capacity can benefit from active (interaction) and passive (viscosity and viscoelastic) contributions.[73,80] We observed that even though the viscosity decreased noticeably, the mean settling velocity did not decrease in the same proportion (Fig. 4–6 and Fig. 9–10). We used an Oakton CON 6+ Handheld Conductivity Meter to measure the conductivity. Before the test, the probe was first calibrated with the 1412 μS cm^{-1} conductivity solution from Ricca Chemical Company which has close conductivity with the measured DBC, DBC and sand. Since the effective electrical conductivity of the colloid suspension depended on complicated factors such as electrical double layer, volume fraction, ionic concentrations and other physicochemical characteristic. The conductivity of DBC, DBC and sand changed in a complex fashion with pH.[87]

Hence, we can deduce that the favorable electrostatic interactions between DBC and sand (active contributions) plays an important role in leading to a superior carrying capacity of sand for DBC formulations. Furthermore, the existence of a networked structures with a characteristics mesh spacing smaller than the proppant size can also give rise to a better ability to retain and hold proppant within a viscosifier gel.[88]

Conclusions

In this work, we demonstrate that the dynamic complexation of diethylenetriamine (DTA) and zwitterionic octadecylamidopropyl betaine (OAPB) can yield a novel type of supramolecular gel with a highly adjustable viscosity characteristic (*i.e.*, pH-responsive supramolecular gel). Such supramolecular assemblies are featured with long, microscale tubules, which have much larger diameter compared to wormlike micelles. These characteristics of DBCs are accompanied with high tolerance against temperature and salinity, making them attractive candidates for hydraulic fracturing applications. Furthermore, the on-demand adjustability of viscosity and precise-control over assembly and disassembly with pH is also important for precisely manipulating proppant injection and deposition into and onto fissures and separation from water. Due to dynamic nature of these supramolecular gels, the permeation damage related problems occurring in traditional linear gels and crosslinked gels may be overcome. Compared to slickwater

(polyacrylamide-based fracturing fluids), the proppant carrying capacity of DBCs is improved about 8- to 73-fold. Based on microstructural analysis and zeta potential studies, the superior proppant carrying capacity of DBCs are ascribed to the synergistic combination of active and passive colloidal retention mechanisms of DBCs. Overall, dynamic supramolecular gels constitute an intriguing class of viscosifiers for hydraulic fracturing application.

Author contributions

Project was conceived by Mustafa Akbulut, Yu-Ting Lin and Shuhao Liu. Experiments were designed by Mustafa Akbulut, Yu-Ting Lin and Shuhao Liu. Laboratory work by Yu-Ting Lin and Shuhao Liu. Data analysis was performed by Mustafa Akbulut, Yu-Ting Lin and Shuhao Liu. NMR work was carried out by Kai-Yuan Kuan. Manuscript was written by Mustafa Akbulut, Yu-Ting Lin and Shuhao Liu and edited by Mustafa Akbulut, Shuhao Liu, Yu-Ting Lin, Bhargavi Bhat, and Joseph Kwon.

Conflicts of interest

The authors declare that there is no conflict of interest.

Acknowledgements

This material is based upon work supported by the U.S. Department of Energy, Office of Fossil Energy under award number DE-FE0031778.

Notes and references

1 U.S. Energy Information Administration, *Dep. Energy*, 2021, pp. 1–6, https://www.eia.gov/energyexplained/us-energy-facts/.
2 B. Looney, *Statistical Review of World Energy*, 2020, vol. 69, p. 66.
3 T. R. S. Oil, V. A. Kuuskraa, S. H. Stevens and K. Moodhe, *Shale Gas Resources: An Assessment of 137 Shale Formations in 41 Countries Outside the United States*, Independent Statistics & Analysis and US Department of Energy, Washington, 2013.
4 U. S. E. I., *Administration,Hydraulically fractured wells provide two-thirds of U.S. natural gas production*, 2016, pp. 1–2, https://www.eia.gov/todayinenergy/detail.php?id=26112.
5 I. H. S. G. Insight, *Hydraulic fracturing accounts for about half of current U.S. crude oil production*, https://www.eia.gov/todayinenergy/detail.php?id=25372.
6 Shale gas production drives world natural gas production growth, https://www.eia.gov/todayinenergy/detail.php?id=27512, accessed January 2021.
7 C. Clark, A. Burnham, C. Harto, R. Horner, *Hydraulic fracturing and shale gas production: technology, impacts, and policy*, Argonne Natl. Lab., 2012, pp. 1–16.
8 H. Hofmann, T. Babadagli and G. Zimmermann, *J. Energy Resour. Technol.*, 2014, **136**, DOI: 10.1115/1.4028690.
9 C. Yegin, M. Zhang, J. V. J. V. Talari and M. Akbulut, *J. Pet. Sci. Eng.*, 2016, **145**, 600–608.
10 H. O. Baled and I. K. Gamwo, in *Thermophysical Properties of Complex Materials*, IntechOpen, 2019.
11 F. Chen, Y. Wu, M. Wang and R. Zha, *Colloid Polym. Sci.*, 2015, **293**, 687–697.
12 J. Gao, G. Zhang, L. Wang, L. Ding, H. Shi, X. Lai, X. Wen, S. Ma and C. Huang, *RSC Adv.*, 2019, **9**, 15246–15256.
13 S. Zhang, Y. She and Y. Gu, *J. Chem. Eng. Data*, 2011, **56**, 1069–1079.
14 Q. Wang, Y. Dan and X. G. Wang, *J. Macromol. Sci., Part A: Pure Appl.Chem.*, 1997, **34**, 1155–1169.
15 A. O. Aliu, J. Guo, S. Wang and X. Zhao, *J. Nat. Gas Sci. Eng.*, 2016, **32**, 491–500.
16 Q. Huang, S. Liu, G. Wang, B. Wu, Y. Yang and Y. Liu, *Fuel*, 2019, **251**, 30–44.
17 R. Barati and J. T. Liang, *J. Appl. Polym. Sci.*, 2014, **131**, 1–11.
18 Y. Chai, X. Li and D. Jing, *Oil Gas Res.*, 2019, **5**, 1.
19 J. Mao, H. Zhang, W. Zhang, J. Fan, C. Zhang and J. Zhao, *J. Ind. Eng. Chem.*, 2018, **60**, 133–142.
20 B. L. Gall, A. R. Sattler, D. R. Maloney and C. J. Raible, *Permeability damage to natural fractures caused by fracturing fluid polymers*, Sandia National Labs., Albuquerque, NM (USA), National Inst. for Petroleum, 1988.
21 C. Yang, Z. Song, J. Zhao, Z. Hu, Y. Zhang and Q. Jiang, *Colloids Surf., A*, 2017, **523**, 62–70.
22 T. Imae, R. Kamiya and S. Ikeda, *J. Colloid Interface Sci.*, 1985, **108**, 215–225.
23 S. Ikeda, S. Hayashi and T. Imae, *J. Phys. Chem.*, 1981, **85**, 106–112.
24 H. Lu, L. Wang and Z. Huang, *RSC Adv.*, 2014, **4**, 51519–51527.
25 M. Zhao, Z. Gao, C. Dai, X. Sun, Y. Zhang, X. Yang and Y. Wu, *J. Surfactants Deterg.*, 2019, **22**, 587–595.
26 W. Kang, P. Wang, H. Fan, H. Yang, C. Dai, X. Yin, Y. Zhao and S. Guo, *Soft Matter*, 2017, **13**, 1182–1189.
27 P. Wang, W. Kang, H. Yang, X. Yin, Y. Zhao, Z. Zhu and X. Zhang, *RSC Adv.*, 2017, **7**, 37699–37705.
28 Z. H. Chieng, M. E. Mohyaldinn, A. M. Hassan and H. Bruining, *Polymers*, 2020, **12**, 1–19.
29 X. Sun, X. Liang, S. Wang and Y. Lu, *J. Pet. Sci. Eng.*, 2014, **119**, 104–111.
30 G. Wang, T. Huang, S. Yan and X. Liu, *J. Mol. Liq.*, 2019, **295**, 111715.
31 H. Xie, M. Asad Ayoubi, W. Lu, J. Wang, J. Huang and W. Wang, *Sci. Rep.*, 2017, **7**, 1–6.
32 A. Baruah, D. S. Shekhawat, A. K. Pathak and K. Ojha, *J. Pet. Sci. Eng.*, 2016, **146**, 340–349.
33 C. Dai, J. Zhao, L. Yan and M. Zhao, *J. Appl. Polym. Sci.*, 2014, **131**, 1–7.
34 S. J. Mushi, W. Kang, H. Yang, P. Wang and X. Hou, *J. Mol. Liq.*, 2020, **301**, 112485.
35 W. Zhang, J. Mao, X. Yang, H. Zhang, J. Zhao, J. Tian, C. Lin and J. Mao, *Chem. Eng. Sci.*, 2019, **207**, 688–701.
36 Y. Wang, Y. Zhang, X. Liu, J. Wang, L. Wei and Y. Feng, *J. Surfactants Deterg.*, 2014, **17**, 295–301.
37 S. M. S. Hussain, L. T. Fogang and M. S. Kamal, *J. Mol. Struct.*, 2018, **1173**, 983–989.

38 H. Wei, R. Zhang, Z. Lei and L. Dang, *Trans. Tianjin Univ.*, 2020, 1–11.
39 J. Yang and J. Hou, *Colloids Surf., A*, 2020, **602**, 125098.
40 D. Feng, Y. Zhang, Q. Chen, J. Wang, B. Li and Y. Feng, *J. Surfactants Deterg.*, 2012, **15**, 657–661.
41 I. C. Chen, C. Yegin, M. Zhang and M. Akbulut, *SPE J.*, 2014, **19**, 1035–1046.
42 G. V Lowry, R. J. Hill, S. Harper, A. F. Rawle, C. O. Hendren, F. Klaessig, U. Nobbmann, P. Sayre and J. Rumble, *Environ. Sci.: Nano*, 2016, **3**, 953–965.
43 A. Shukla and H. Rehage, *Langmuir*, 2008, **24**, 8507–8513.
44 M. Ibrahim, A. Nada and D. E. Kamal, *Indian J. Pure Appl. Phys.*, 2005, **43**, 911–917.
45 S. Liu, J. Zheng, L. Hao, Y. Yegin, M. Bae, B. Ulugun, T. M. Taylor, E. A. Scholar, L. Cisneros-Zevallos, J. K. Oh and M. Akbulut, *ACS Appl. Mater. Interfaces*, 2020, **12**, 21311–21321.
46 L. Carolei and I. G. R. Gutz, *Talanta*, 2005, **66**, 118–124.
47 L. Hao, C. Yegin, J. V Talari, J. K. Oh, M. Zhang, M. M. Sari, L. Zhang, Y. Min, M. Akbulut and B. Jiang, *Soft Matter*, 2018, **14**, 432–439.
48 P. A. Dantas and V. R. Botaro, *Open J. Polym. Chem.*, 2012, **02**, 144–151.
49 Y. L. Chen, L. Zhang, J. Song, G. Jian, G. Hirasaki, K. Johnston and S. L. Biswal, *Langmuir*, 2019, **35**, 695–701.
50 Y. Li, M. Puerto, X. Bao, W. Zhang, J. Jin, Z. Su, S. Shen, G. Hirasaki and C. Miller, *J. Surfactants Deterg.*, 2017, **20**, 21–34.
51 C. P. Baryiames, M. Teel and C. R. Baiz, *Langmuir*, 2019, **35**, 11463–11470.
52 S. J. Mushi, W. Kang, H. Yang, P. Wang and X. Hou, *J. Mol. Liq.*, 2020, **301**, 112485.
53 C. Zhou, X. Cheng, O. Zhao, S. Liu, C. Liu, J. Wang and J. Huang, *Soft Matter*, 2014, **10**, 8023–8030.
54 I. N. Alves, *SPE Prod. Eng.*, 1992, 363–367.
55 H. Hofmann, T. Babadagli and G. Zimmermann, *Appl. Energy*, 2014, **113**, 524–547.
56 A. H. Abdel-Alim and A. E. Hamielec, *J. Appl. Polym. Sci.*, 1973, **17**, 3769–3778.
57 A. M. Mansour, R. S. Al-Maamari, A. S. Al-Hashmi, A. Zaitoun and H. Al-Sharji, *J. Pet. Sci. Eng.*, 2014, **115**, 57–65.
58 H. Y. Lee, S. H. Park, J. H. Kim and M. S. Kim, *Polym. Chem.*, 2017, **8**, 6606–6616.
59 J. Y. Seo, B. Lee, T. W. Kang, J. H. Noh, M. J. Kim, Y. B. Ji, H. J. Ju, B. H. Min and M. S. Kim, *Tissue Eng. Regener. Med.*, 2018, **15**, 513–520.
60 H. A. Nasr-El-Din, A. H. Al-Ghamdi, A. A. Al-Qahtani and M. M. Samuel, *SPE J.*, 2008, **13**, 35–47.
61 W. Al-Sadat, M. S. Nasser, F. Chang, H. A. Nasr-El-Din and I. A. Hussein, *J. Pet. Sci. Eng.*, 2014, **122**, 458–467.
62 B. Wu, X. Wang, J. Yang, Z. Hua, K. Tian, R. Kou, J. Zhang, S. Ye, Y. Luo, V. S. J. Craig, G. Zhang and G. Liu, *Sci. Adv.*, 2016, **2**, e1600579.
63 S. Sathivel, J. Huang and W. Prinyawiwatkul, *J. Food Eng.*, 2008, **84**, 187–193.
64 C. Du and R. J. Hill, *J. Rheol.*, 2019, **63**, 109–124.
65 R. G. Shrestha, L. K. Shrestha and K. Aramaki, *J. Colloid Interface Sci.*, 2008, **322**, 596–604.
66 N. A. Razak and M. N. Khan, *Rheol. Acta*, 2013, **52**, 927–937.
67 F. J. Millero, R. Feistel, D. G. Wright and T. J. McDougall, *Deep Sea Res., Part I*, 2008, **55**, 50–72.
68 L. Zeng, N. Reid, Y. Lu, M. M. Hossain, A. Saeedi and Q. Xie, *Energy Fuels*, 2020, **34**, 3031–3040.
69 A. Khatory, F. Lequeux, F. Kern and S. J. Candau, *Langmuir*, 1993, **9**, 1456–1464.
70 K. Vogtt, G. Beaucage, M. Weaver and H. Jiang, *Soft Matter*, 2017, **13**, 6068–6078.
71 A. Maghzi, R. Kharrat, A. Mohebbi and M. H. Ghazanfari, *Fuel*, 2014, **123**, 123–132.
72 V. Adibnia, G. Afuwape and R. J. Hill, *Macromolecules*, 2020, **53**, 7460–7468.
73 D. Dogon and M. Golombok, *J. Unconv. Oil Gas Resour.*, 2016, **14**, 12–21.
74 N. Yekeen, E. Padmanabhan and A. K. Idris, *J. Ind. Eng. Chem.*, 2018, **66**, 45–71.
75 Y. Zhao, S. J. Haward and A. Q. Shen, *J. Rheol.*, 2015, **59**, 1229–1259.
76 F. E. Critchfield and J. B. Johnson, *Anal. Chem.*, 1959, **31**, 570–572.
77 M. P. Applebey, *J. Chem. Soc., Trans.*, 1910, **97**, 2000–2025.
78 W. fen Pu, D. jun Du and R. Liu, *J. Pet. Sci. Eng.*, 2018, **167**, 568–576.
79 C. A. Dreiss, *Soft Matter*, 2007, **3**, 956–970.
80 J. Mao, X. Yang, D. Wang, Y. Li and J. Zhao, *RSC Adv.*, 2016, **6**, 88426–88432.
81 X. Pei, J. Zhao, Y. Ye, Y. You and X. Wei, *Soft Matter*, 2011, **7**, 2953–2960.
82 P. S. Patel, C. J. Robart, M. Ruegamer and A. Yang, *Soc. Pet. Eng. - SPE Hydraul. Fract. Technol. Conf.* 2014, vol. 2014, pp. 854–873.
83 C. A. J. Blyton, D. P. Gala and M. M. Sharma, *SPE Drill. Completion*, 2018, **33**, 307–323.
84 A. W. Coulter Jr, E. K. Frick and M. L. Samuelson, in *SPE Annual Technical Conference and Exhibition*, Society of Petroleum Engineers, 1983.
85 S. Wang, Y. Zhang, J. Guo, J. Lai, D. Wang, L. He and Y. Qin, *J. Pet. Sci. Eng.*, 2014, **124**, 432–435.
86 N. V Thampi, R. P. John, K. Ojha and U. G. Nair, *Ind. Eng. Chem. Res.*, 2016, **55**, 5805–5816.
87 M. F. Zawrah, R. M. Khattab, L. G. Girgis, H. El Daidamony and R. E. A. Aziz, *HBRC J.*, 2016, **12**, 227–234.
88 S. Chen and J. P. Rothstein, *J. Non-Newtonian Fluid Mech.*, 2004, **116**, 205–234.
89 S. Paharo, B. Bhadriraju, M. Akbulut and J. S. Kwon, *J. Colloid Interface Sci.*, 2021, **600**, 550–560.
90 S. Pahari, P. Bhandakkar, M. Akbulut and J. S. Kwon, *Energy*, 2021, **216**, 119231.